Eur. Phys. J. B **61**, 83–88 (2008)
DOI: 10.1140/epjb/e2008-00030-4

THE EUROPEAN PHYSICAL JOURNAL B

Can a difference in molecular weights cause an eruption in a driven flow of self-organizing immiscible system?

R.B. Pandey[1,2,a] and J.F. Gettrust[1]

[1] Naval Research Laboratory, Stennis Space Center, MS 39529, USA
[2] Department of Physics and Astronomy University of Southern Mississippi, Hattiesburg, MS 39406-5046, USA

Received 1st August 2007 / Received in final form 27 November 2007
Published online 23 January 2008 –

Abstract. Driven flow of a non-equilibrium non-conservative (NENC) system with a mixture of immiscible particles (A, B of molecular weight M_A, M_B) exhibits self-organizing patterns (segregation, phase-separation, etc.) in steady-state. The flow response (v) of mass flux density (j) to bias (H), $v = \partial j/\partial H$ in steady-state is found to be sensitive to molecular weight ratio ($\alpha = M_B/M_A$). While the flux density (j) responds linearly to bias for both components (A, B) at $\alpha = 1$, onset of eruptive response occurs at extreme bias ($H \to 1$) at $\alpha > 1$ where $v \to \infty$ for heavier (B) and $v \to -\infty$ for lighter (A) constituents. Difference in molecular weights (M_A, M_B) is not only critical to eruptive flow but also in controlling the flow response prior to this crossover.

PACS. 61.43.Bn Structural modeling: serial-addition models, computer simulation – 83.10.Rs Computer simulation of molecular and particle dynamics

Understanding the morphological evolution, transport, and flow [1–23] of particle systems have attracted enormous attention recently due to their response to external bias particularly in granular systems [1–18]. Systems modeled by coarse-grained particles have diverse variations in spatial and temporal scales, i.e., nano-scale materials in laboratory to large scale applications such as flow of water and sand mixtures, dissociation of methane and hydrocarbon below the ocean floor [24–28], and mud volcanoes. One would expect interesting responsive phenomena in the flow of dissimilar constituents [29–31] which are not generally captured by traditional hydrodynamic methods. Computer simulations with particles are very useful in understanding the evolution of global patterns from microscopic details. A range of computational methods are employed in such studies including lattice gas [19,20], molecular dynamics [18,21,22], and Monte Carlo [23] methods. Number of particles (constituents) is conserved in computational modeling of most granular systems which is applicable to a range of systems [1–18] in equilibrium. In many driven systems including formation and dissociation of methane hydrate and mud volcanoes, the number of particles is not conserved. Non-equilibrium steady-state systems [32,33] with non-conserved constituents exhibit interesting flow response and structural patterns [29–31].

Flow properties of particulate systems are frequently studied by a number of lattice gas methods [34–36]. It is, however, easier to incorporate interactions between constituent particles and effective medium (empty lattice sites, see below) in interacting lattice gas [32,33] than that with the widely used Boltzmann lattice gas [34,35] in studying the flow. Using an interacting lattice gas model [29–31], we study the flow response of an immiscible mixture with dissimilar components A and B driven by a pressure bias (H) against sedimentation. For a specific molecular weight ratio, we have recently observed [31] an eruptive flow response at the extreme value of the bias. It is not clear how such a quantity as the difference in molecular weight ratio affect the response. In this article we show that the difference in molecular weights of dissimilar constituents is not only key to eruptive response but also in orchestrating the flow response prior to its divergence at the extreme bias.

We consider a mixture of two components A and B (each with molecular weight M_A and M_B) on a cubic lattice of size L^3 with $L = 30$–200. Almost all data presented here are generated on 100^3 sample. Different sample sizes are, however, used to check for the finite size effects. No severe finite size effect is observed on the qualitative behavior unless specified otherwise. The molecular weight ratio $\alpha = M_B/M_A$ is varied with $M_A = 0.1$ and $\alpha = 1 - 10$. Particles A and B are randomly distributed initially at about 50% of the lattice sites with one particle at a site.

[a] e-mail: ras.pandey@usm.edu

A nearest neighbor interaction between particles (A, B) and empty (pore) sites (O) is described by the energy,

$$E_i = \sum_k \sum_n J(k, n) \tag{1}$$

where index k runs over all sites occupied by particles and n over all nearest neighbor sites of k. The interaction matrix elements,

$$J(A, A) = J(B, B) = -J(A, B) = -J(B, A) = -\epsilon;$$
$$J(A, O) = J(B, O) = -1. \tag{2}$$

The interaction strength or miscibility gap $\epsilon = 1$. Molecular weights of constituents affect their sedimentation. The gravitational potential energy E_g of a particle at height z (in unit of g, the acceleration due to gravity) is given by

$$E_g = M_{A/B}\ z. \tag{3}$$

The sedimentation probability is coupled with the change in gravitational potential energy via the Boltzmann distribution (see below).

A source of particles is connected to the bottom plane $(z = 1)$. This causes a concentration gradient (see below) which exerts a driving force upward. Additionally, the hydrostatic pressure bias (H) pushes fluid constituents upward $(+z$ direction) against the gravitational sedimentation downward $(-z$ direction). The bias is implemented in selecting one of the nearest neighbor sites along $\pm x, \pm y, \pm z$ directions with probabilities,

$$P_x = P_{-x} = P_y = P_{-y} = \frac{1}{6};$$
$$P_z = \frac{1+H}{6}, P_{-z} = \frac{1-H}{6};\ 0 \le H \le 1. \tag{4}$$

Attempts are made to move each randomly selected particle (A and B) to their nearest neighbor sites chosen with the bias probability H with the Metropolis algorithm. Following procedure is used to implement the algorithm. A particle is selected randomly say at site i and one of its nearest neighbor site j is selected with the bias probability H. If the site j is already occupied by another particle, then the attempt to move the particle fails. If the site j is empty, then the particle is moved (from the site i to site j) with the Boltzmann probability $e^{-\Delta E/\tau}$ where ΔE is the change in energy $E = E_i + E_g$ due to move and τ is the temperature in unit of Boltzmann constant and energy; $\tau = 1$ is used in this study. When a particle at the bottom plane $(z = 1)$ moves horizontally (xy-plane) or upward (to $z = 2$ plane), a new particle (A or B) from the source is released into the vacated site according to its current lattice concentration as described before [29–31]. The cubic box is open along vertical boundaries, i.e., a particle can drop out when it attempts to move down from the bottom or escape from the top $(z = L)$. Periodic boundary conditions are implemented along the transverse (x, y) directions. An attempt to move each particle once defines unit Monte Carlo step (MCS) time.

The number and densities of particles and their distributions change as the simulation proceeds. Release of particles from the source at the bottom leads to a net flow along the longitudinal (z) direction. The competing driving fields due to pressure bias and gravity further affect the flow and pattern. A steady-state is reached with a stable density profile and a constant rate of mass flux in the asymptotic time limit. The simulation is repeated for a number of independent samples to obtain a reliable estimate of physical quantities. These quantities include, root mean square (rms) displacement of tracers (particles) and that of their center of mass, density profiles (longitudinal and transverse), correlation profiles (i.e., average number of different neighbors of each particles), flow rate and flux rate density, etc. as a function of the bias H for different values of molecular weight ratios α. We have already studied the structural response, i.e., density profiles of A and B and their steady-state concentrations [29]. In this article, we constrain to flux response.

Figure 1 shows a typical snap-shot of particles. It is clear to see segregation and phase separation with dense phase toward the lower part and low density toward the top. As mentioned above, the number of constituents is not conserved. Therefore, both the number of particles and density profiles evolve with the time step as shown in Figure 2 for a molecular weight ratio $\alpha = 10$ at high values of bias $H = 0.7$–1.0. Initially the total number (N_A) of A particles in the lattice decreases while the number (N_B) of B particles increases with the time steps. Both N_A and N_B attain almost constant values in steady-state equilibrium with $N_B > N_A$.

The equilibrium values of N_A and N_B depend non-monotonically on the pressure bias [29]. The steady-state density (of B are larger than that of A) profiles show non-linear including sigmoidal variation (see below) along the longitudinal direction (from bottom to top). The driving force due to concentration gradient is thus non-linear along the longitudinal direction as pointed out before [29]. A self-organizing morphology with a stable structural pattern is however achieved at each bias and molecular weight ratio even though there is a constant mobility of particles from bottom to top. At high pressure bias and large molecular weight ratio $(\alpha = 10)$, the density profile is overwhelmingly dominated by the heavier (B) particles with a relatively uniform distribution along the transverse direction (Fig. 2).

The transverse density profiles provide insight into the complementary structural patterns. For example, the spatial complementary oscillation in transverse density profiles of A and B reveals a phase separation or de-segregation [29] at low bias $H = 0.1$ (Fig. 3). Segregation (Fig. 3) reduces considerably on increasing the bias and almost vanishes at high values of the bias (Fig. 2) where the driving bias dominates over the interaction energy $(E = E_i + E_g)$. The difference in density (higher with higher molecular weight) is however increases with the bias. In general, increasing the pressure bias reduces the non-linearity [29] in the longitudinal density profiles and smears out the contrast (amplitude of oscillations) in phase separation seen from the transverse density profiles (Fig. 3). These structural patterns affect the flow (follows).

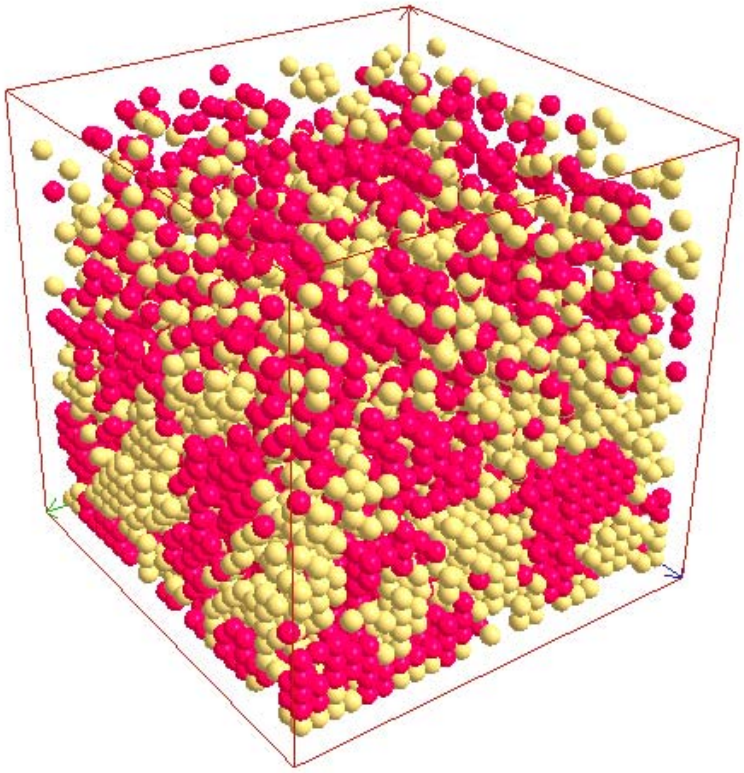

Fig. 1. Immiscible A (light, $M_A = 0.1$) and B (dark, $M_B = 0.3$) particles with pressure bias $H = 0.4$ at time steps $t = 1000$ on a 25^3 lattice with $\epsilon = 1$.

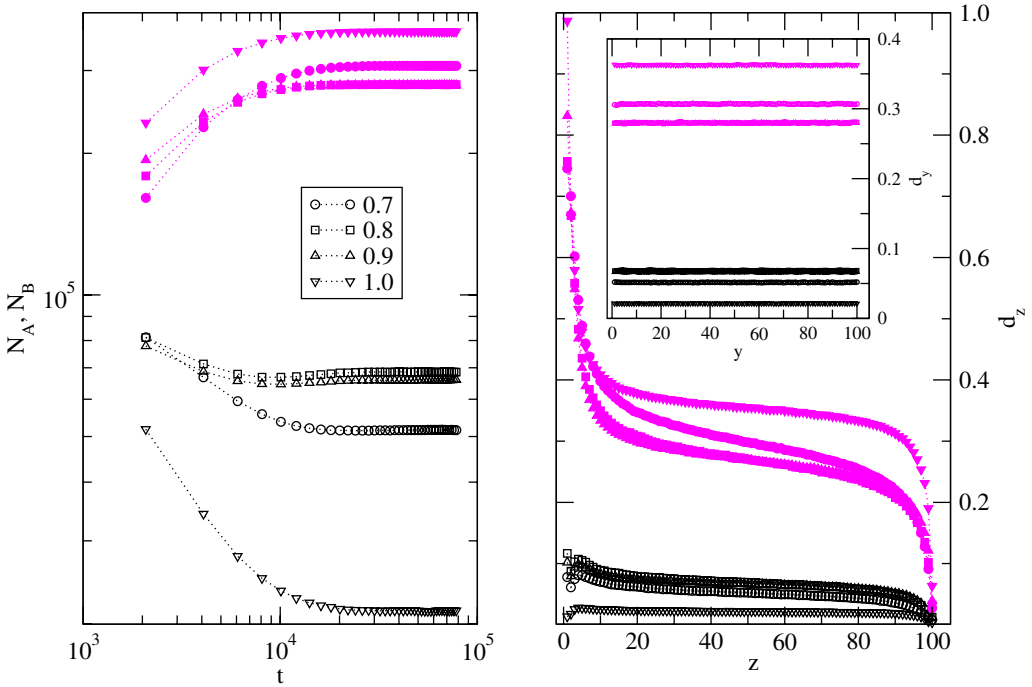

Fig. 2. Left: number of particles (N_A, N_B) versus time steps at bias $H = 0.7$–1.0 with their molecular weights $M_A = 0.1$ and $M_B = 1.0$. A (open, black) and B (filled) symbols. Right: longitudinal (z) and transverse (y) (inset) density profiles in steady-state. Sample size 100^3 with 128 independent runs.

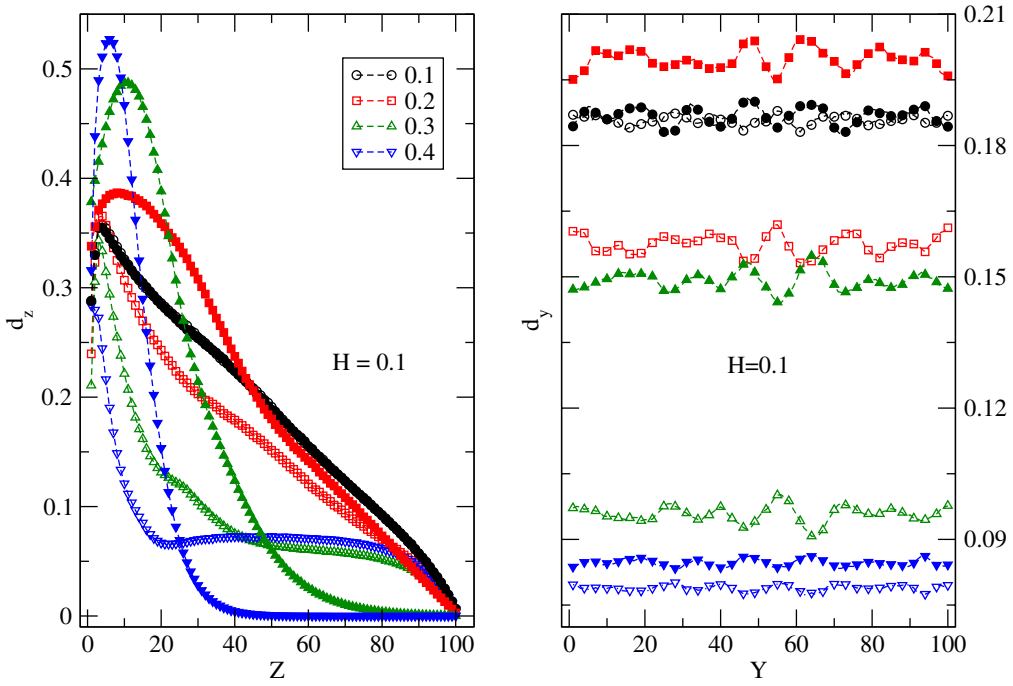

Fig. 3. Density profile of A (open) and B (filled) at bias $H = 0.1$ for their molecular weights $M_A = 0.1$ and $M_B = 0.1 - 0.4$. Left: longitudinal (z) and right: transverse (y) density profiles in steady-state. Sample size 100^3 with 128 independent runs.

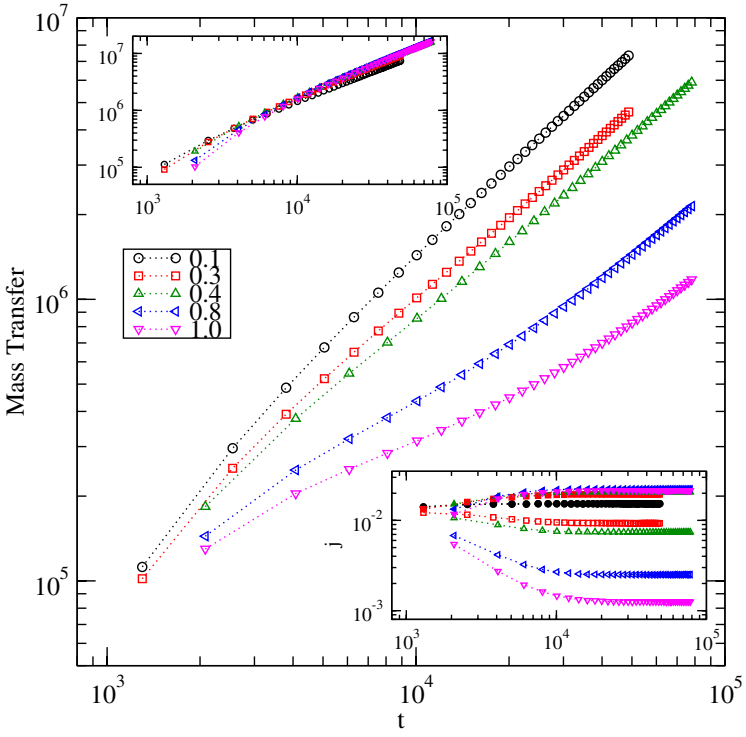

Fig. 4. Net mass transfer along longitudinal direction of A and B (top inset) and corresponding flux density (j) versus time steps at bias $H = 1.0$ for $M_A = 0.1$ and $M_B = 0.1, 0.3, 0.4, 0.8, 1.0$. As many as 128 independent samples are used on 100^3 lattice.

Obviously, there is a net flow of A and B from bottom to top. Evolution of the mass flux with the time step is presented in Figure 4. The mass transfer Q of each component increases linearly with the time steps in the asymptotic long time regime which indicates that the system has reached a steady-state. Corresponding current (flux) density j can be evaluated from

$$j = \frac{1}{L_x \times L_y} \frac{dQ}{dt}. \quad (5)$$

Evolution of j shows how it reaches a constant value for each molecular weight ratio. The constant value of the flux density implies that the dynamic system has reached the steady-state which is also consistent with a stable morphology. Thus, both structure and flow become stable in the asymptotic time regime. It is important to point out that the unit of time is arbitrary similar to energy and molecular weight which is a common practice in such a coarse-grained modeling with phenomenological interactions. However, the time step appears to scale linearly

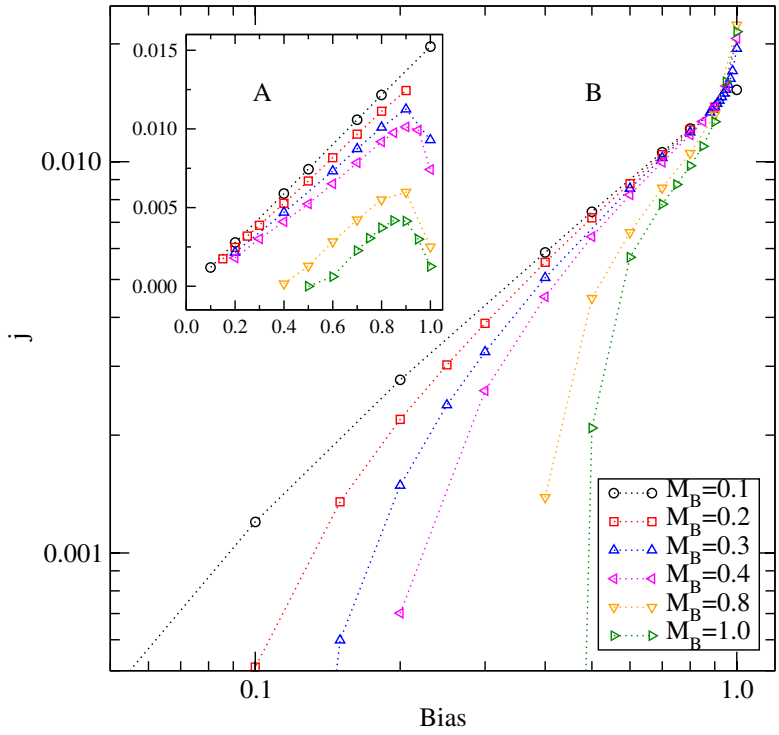

Fig. 5. Steady-state flux density (j) of A and B versus bias H for $M_A = 0.1$ and $M_B = 0.1$–1.0. As many as 128 independent samples are used on 100^3 lattice.

with a realistic time frame born out by the linear mass flow expected from the solution of a simple driven diffusive system [37]. Our goal is to understand trends in the flow response with respect to variations in parameters such as pressure bias and molecular weight.

How does the steady-state flux density ($j_{A/B}$) respond to pressure bias for mixtures of different molecular weight ratios? Figure 5 shows the variation of the flux density with the pressure bias for various mixtures, $\alpha = M_B/M_A = 1$–10. For a symmetric molecular weight ratio ($\alpha = 1$), we see a linear response throughout the pressure bias regime. On increasing the molecular weight ratio, the flux density response of A and B begin to differ. At low bias the flux density response of both component is linear (which is better seen in the normal plot, the inset figure than on the log-log plot). At large values of bias, the response becomes non-linear. The response of higher molecular weight ($M_B = 0.2$–1.0) component diverges while that of lower weight component (A) declines dramatically at extreme values of the bias. Let us define a volatility index,

$$v = \partial j/\partial H. \tag{6}$$

We see that $v \to \infty$ for B and $v \to -\infty$ for A as $H \to 1$.

What happens when a difference in the molecular weight of particles A and B sets in that causes an eruptive flow response of the heavier (B) component? We have already seen such an eruptive response for a fixed value of $\alpha = 3$ [31]. The variation of the molecular weight ratio (α) as presented here, however, shows that (i) the difference in molecular weight is the root cause of eruptive response (which vanishes for $\alpha = 1$), (ii) approach to eruptive flow differ considerably with the difference in molecular weight of the constituents – larger the difference, the faster is the response (v) of the heavier component prior to eruption, and (iii) the nature of eruption remains independent of the molecular weight ratio ($\alpha > 1$) as $H \to 1$. Asymmetry in the molecular weights of the constituents seems to introduce correlation between the source and the dynamic lattice system. Particularly, the correlation among particles with the higher molecular weight increases on increasing the bias leading to eruption in their flow while an opposite trend occurs concurrently in flow of the component with the lower molecular weight.

We acknowledge partial support from ONR PE # 0602435N and NSF-EPSCoR grants. This work was supported in part by grants of computer time from the DOD High Performance Computing Modernization Program at the Major Shared Resource Center (MSRC), NAVO, Stennis Space Center.

References

1. B. Behringer, Nature **415**, 594 (2002)
2. E.I. Corwin, H.M. Jaeger, S.R. Nagel, Nature **435**, 1075 (2005)
3. M.P. Ciamarra, A. Coniglio, M. Nicodemi, Phys. Rev. Lett. **94**, 188001 (2005)
4. P. Sanchez, M.W. Swift, P.J. King, Phys. Rev. Lett. **93**, 184302 (2004)
5. S.R. Hutton, A.J. Forsyth, M.J. Rhodes, C.F. Osborne, Phys. Rev. E **70**, 031301 (2004)
6. H.-Q. Wang, G.-J. Jin, Y.-Q. Ma, Phys. Rev. E **68**, 031301 (2003)

7. J. Chakrabarti, J. Dzubiella, H. Lowen, Europhys. Lett. **61**, 415 (2003)
8. J. Rajchenbach, Phys. Rev. Lett. **90**, 144302 (2003)
9. B. Meerson, T. Poschel, Y. Bromberg, Phys. Rev. Lett. **91**, 024301 (2003)
10. J.-C. Tsai, G.A. Voth, J.P. Gollub, Phys. Rev. Lett. **91**, 064301 (2003)
11. T. Mullin, Phys. Rev. Lett. **84**, 4741 (2000)
12. J. Dzubiella, G.P. Hoffmann, H. Lowen, Phys. Rev. E **65**, 021402 (2002)
13. *Granular Matter: An Interdisciplinary Approach*, edited by A. Mehta (Springer, New York, 1994)
14. *Unifying Concepts In Granular Media And Glasses*, edited by A. Coniglio, A. Fierro, H.J. Herrmann, M. Nicodemi (Elsevier, 2004)
15. H.A. Makse, S. Havlin, P.R. King, H.E. Stanley, *Novel Pattern Formation in Granular Matter*, edited by L. Schimansky-Geier, T. Poeschel (Springer, Heidelberg, 1997), p. 319
16. H.A. Makse, Physica A **330**, 83 (2003)
17. M. Latzel, S. Luding, H.J. Herrmann, Granular Matter **2**, 123 (2000)
18. D.C. Rapaport, Phys. Rev. E **65**, 61306 (2002)
19. A. Xu, G. Gonnella, A. Lamura, Physica A **331**, 10 (2004)
20. L.O.E. Santos, P.C. Facin, P.C. Philippi, Phys. Rev. E **68**, 056302 (2003)
21. M.C. Mitchell, J.D. Autry, T.M. Nenoff, Molecular Phys. **99**, 1831 (2001)
22. G. Foffi, W. Gotze, F. Sciortino, P. Tartaglia, Th. Voigtmann, Phys. Rev. E **69**, 011505 (2004)
23. R. Finken, J.P. Hansen, A.A. Louis, J. Phys. A: Mathematical and General **37**, 577 (2004)
24. E.D. Sloan, *Clathrate Hydrates of Natural Gases*, 2nd edn. (Marcel Dekker, New York, 1997)
25. *Proceeding of the Fourth International Conference on Gas Hydrate* (Yokohama, 2002)
26. W.T. Wood, J.F. Gettrust, in *Natural Gas Hydrates: Occurence, Distribution, and Dynamics*, edited by C.K. Paull, W.P. Dillon (AGU Monograph 124, 2001), p. 165
27. Chuang Ji, G. Ahmadi, W. Zhang, D.H. Smith in [25], p. 791
28. Hisashi O. Kono, B. Budhijanto, S. Narasimhan, D.H. Smith in [25], p. 543
29. R.B. Pandey, J.F. Gettrust, Physica A **345**, 555 (2005)
30. R.B. Pandey, J.F. Gettrust, Physica A **358**, 437 (2005)
31. R.B. Pandey, J.F. Gettrust, Physica A **368**, 416 (2006)
32. B. Schmittmann, R.K.P. Zia, *Statistical Mechanics of Driven Diffusive Systems* (Academic Press, 1995)
33. Y. He, R.B. Pandey, Phys. Rev. Lett. **71**, 565 (1993)
34. D.H. Rothman, S. Zaleski, *Lattice-Gas Cellular Automata Simple Models of Complex Hydrodynamics* (Cambridge University Press, 1997)
35. D.A. Wolf-Gladrow, *Lattice Gas Cellular Automata and Lattice Boltzmann Models: An Introduction (Lecture Notes in Mathematics)* (Springer, 2000)
36. S. Succi, *Lattice Boltzmann Equation for Fluid Dynamics and Beyond* (Oxford University Press, 2001)
37. E.L. Cussler, *Diffusion: Mass transfer in fluid systems* (Cambridge University Press, 1984)